LBL-11556

MASTER

CONF-800863--5

Lawrence Berkeley Laboratory

UNIVERSITY OF CALIFORNIA

Presented at the International Conference on Nuclear Physics, Lawrence Berkeley Laboratory, Berkeley, CA, August 24-30, 1980; and published in the Proceedings

CURRENT TOPICS IN RELATIVISTIC NUCLEAR COLLISIONS

Miklos Gyulassy

August 1980

Prepared for the U.S. Department of Energy under Contract W-7405-ENG-48

DISTRIBUTION OF THIS DOCUMENT IS UNLIMITED

DISCLAIMER

CURRENT TOPICS IN RELATIVISTIC NUCLEAR COLLISIONS

Miklos Gyulassy

Nuclear Science Division, Lawrence Berkeley Laboratory
University of California, Berkeley, California 94720, U.S.A.

Abstract: First, we discuss current attempts to deduce the nuclear matter equation of state from inclusive data. Next, some puzzling projectile fragment properties found in emulsions are discussed. Finally, a new test of pion condensation is proposed and current pion data reviewed.

1. Introduction

For this brief overview of relativistic nuclear collisions, I have chosen the following three topics that emphasize the unique aspects of this field:

1. Current attempts to deduce the nuclear matter equation of state, $W(n,\mathcal{T})$, from inclusive data:

$$A + B \overset{?}{\rightarrow} W(n,\mathcal{T}) + X \quad . \tag{1}$$

2. The search for new states of nuclear matter among projectile fragments in emulsions:

$$B + Em \rightarrow B^{*} + Em \rightarrow B^{**} + Em \quad . \tag{2}$$

3. An "almost" test of pion condensation:

$$A + B \rightarrow \text{pions} + X \quad . \tag{3}$$

Obviously, I will not have time to cover the tremendous volume of data and model calculations that have accumulated over the past few years. These data and calculations have played a crucial role in our increased understanding of the basic reaction mechanism of nuclear collisions at ~1 GeV/nucleon. Extensive reviews of the progress made in untangling the complex details of that reaction mechanism can be found in recent conference proceedings[1-4]. However, in addition to offering a rich new domain for reaction mechanism studies, relativistic nuclear collisions offer a unique tool to probe the properties of nuclear matter far outside the domain of conventional nuclear physics. The three topics above focus on this aspect of the field.

The primary motivation for studying nuclear collisions at high energies is shown in fig. 1. This figure, prepared by Gudima and Toneev[5], shows the time evolution of the average density, n/n_o, and temperature, $\mathcal{T}$, as computed via their intranuclear cascade code.

Two typical nuclear reactions are illustrated. The curves demonstrate clearly that for times, $t \sim 3\text{-}5 \times 10^{-23}$ sec, high densities $n \sim (3\text{-}4)n_o$ ($n_o \approx 0.15 fm^{-3}$) along with high temperatures $\mathcal{T} \sim 50\text{-}100$ MeV can be reached in such reactions. To appreciate the significance of this result, recall that for the past 50 years--one-half century--nuclear physicists have concentrated on the rich properties of nuclear matter in the extremely narrow region of the $(n,\mathcal{T})$ plane near the lower left-hand corner. What fig. 1 demonstrates is that we now have a unique tool to expand

DISTRIBUTION

This manuscript was printed from originals provided by the author.

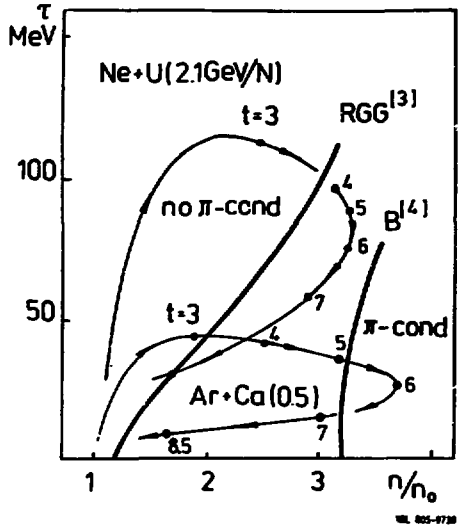

Fig. 1. Temporal evolution (in 10^{-23} sec steps) of average density n and temperature τ via cascade calculations of Gudima and Toneev[5]. Critical temperature $\tau_c(n)$ for pion condensation is given by RGG[10] and B[11].

the domain of nuclear physics into a much larger range of densities and excitation energies. Of course, fig. 1 tells us nothing about how easy or difficult it will be to read off the properties of dense nuclear matter from actual inclusive data. However, the possibility that it might be done mandates that we try.

Nothing is known experimentally about the properties of nuclear matter at high (n,τ). Nevertheless--or consequently--there are intriguing theoretical speculations about exotic phase transitions that might occur under those conditions. Such fun topics as pion condensation[6,7], density isomerism[8] and even quark matter[9] phase transitions have been considered in the literature (see also M. Rho's contribution in these proceedings). For example, in fig. 1 the pion condensation phase boundary is shown from two model calculations. The differences between curves RGG[10] and B[11] indicate typical theoretical uncertainties in such calculations. The point to note is that high enough densities and low enough temperatures could in principle be achieved for the <u>onset</u> of pion condensation. The possible signatures of such a phase transition will be discussed in section 4.

While such exotic possibilities add further incentive to bang nuclei together, the most fundamental property of nuclear matter that we ultimately hope to determine is the nuclear equation of state, $W(n,\mathcal{T})$ = energy per baryon at fixed $(n,\mathcal{T})$. In the next section, our current attempts to determine $W(n,\mathcal{T})$ from inclusive data are discussed.

2. Hydrodynamics, $W(n,\mathcal{T})$, and inclusive data

To connect $W(n,\mathcal{T})$ with data, we need an appropriate theoretical framework. That framework is clearly hydrodynamics[12]). Recall the basic equations of hydrodynamics. These are the continuity of baryon number density n, momentum density $\underset{\sim}{m}$, and energy density e:

$$\frac{\partial}{\partial t}\begin{pmatrix} n \\ \underset{\sim}{m} \\ e \end{pmatrix} + \underset{\sim}{\nabla}\cdot\begin{pmatrix} \underset{\sim}{v}n \\ \underset{\sim}{v}\underset{\sim}{m} \\ \underset{\sim}{v}e \end{pmatrix} = \begin{pmatrix} 0 \\ -\underset{\sim}{\nabla}P \\ -\underset{\sim}{\nabla}\cdot(\underset{\sim}{v}P) \end{pmatrix} , \tag{4}$$

where $\underset{\sim}{v}(\underset{\sim}{x},t)$ is the flow velocity field and $P = n^2\partial W(n,\mathcal{T})/\partial n$ (at constant entropy) is the pressure.

Equation (4) is the simplest form of hydrodynamics when dissipative effects are neglected. Such effects become important when the gradient of some field quantity, $f(x,t)$, is comparable to the mean free path λ. Corrections to eq. (4) to order $\lambda|\nabla f|/f$ lead to the Navier Stokes equations, involving the viscoscity and thermal conductivity transport coefficients[13,14]). First, we discuss the results using eq. (4).

The basic input in eq. (4) is the nuclear equation of state, $W(n,\mathcal{T})$, for which the following assumption on the temperature dependence was made[12,15]):

$$W(n,\mathcal{T}) = W_o(n) + I(n,\mathcal{T}) \quad . \tag{5}$$

The internal energy I is assumed to be of the form appropriate for a nonrelativistic Fermi gas. The pressure in eq. (4) is then given by $P = n^2\partial W_o/\partial n + 2/3\, nI$. In eq. (5), W_o is the compression energy at zero temperature. To test the sensitivity of the results to W_o, three extreme models of W_o were considered as illustrated in fig. 2. The curve for compressibility K = 200 MeV represents a reasonable guess for W_o. Also, a rather stiff equation of state with K = 400 and a very soft equation of state with a density isomer at $3n_o$ were considered.

Before comparing with data, we note that composite fragment production is not correctly treated via hydrodynamics due to poor surface properties of the latter. Thus, the fraction of protons that emerge in composite fragments cannot be calculated in this framework. We can, however, define a <u>charged particle</u> inclusive cross section by summing over the inclusive cross sections, $d\sigma(Z,N)$, for composites with Z protons, N neutrons as follows:

$$\varepsilon\frac{d^3\sigma}{d^3p}\,ch = \sum_{Z,N} Z\varepsilon\,\frac{d^3\sigma}{d^3p}\,(Z,N) \tag{6}$$

where (ε,p) is the same energy-momentum <u>per nucleon</u> for all fragments in the sum. Underlying eq. (6) is the assumption that composite fragments are produced via final state interactions, after the violent phase of the collision. Thus, $d\sigma_{ch}$ is thought to represent the "primordial" distribution of protons, before

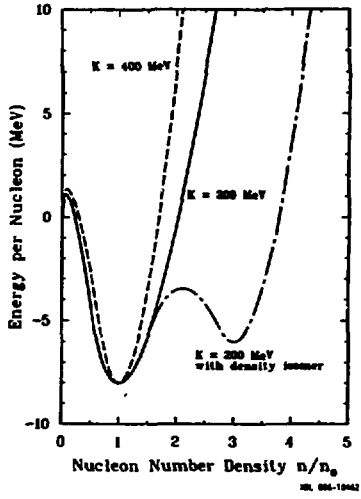

Fig. 2. Three examples of nuclear equation of state $W_o(n)$, eq. (5), considered in Ref. [15]).

coalescence[1-4]) into light composites occurs. With this assumption, the distribution of charges obtained by solving eq. (4) can be compared with the charged particle inclusive data.

The difference between $d\sigma_{ch}$ and $d\sigma(1,0) = d\sigma_p$ is largest for laboratory energies $E \lesssim 50$ MeV and forward angles. It is also important to remember that for heavy systems there can be large Coulomb distortions of the spectra, the magnitude of which is determined by $Z\alpha/RE$. Thus for U targets Coulomb distortion can modify the spectra by over 50% for $E \lesssim 40$ MeV. For $E > 50$ MeV, both composite production and Coulomb effects are not so important, and therefore it is in this region where hydrodynamics should agree best with the data.

For the impact parameter averaged inclusive spectra we see in fig. 3 that the hydrodynamic calculations[15]) provide, in fact, a reasonable description of the data[16]) for $E > 50$ MeV. However, within numerical uncertainties there also appears to be very little sensitivity to the three equations of state (fig. 2) studied. A similar insensitivity of the impact parameter averaged single particle inclusive cross section to the equation of state was found in Ref. 17). The calculations in Ref. 15) still do not include the final thermal averaging for each fluid cell, and only the flow velocities have been used to calculate $d\sigma_{ch}$. In a one dimensional example[15]), thermal averaging was found to reduce the small sensitivity to the equation of state even further. This was also anticipated in Ref. 17). In addition, classical equations of

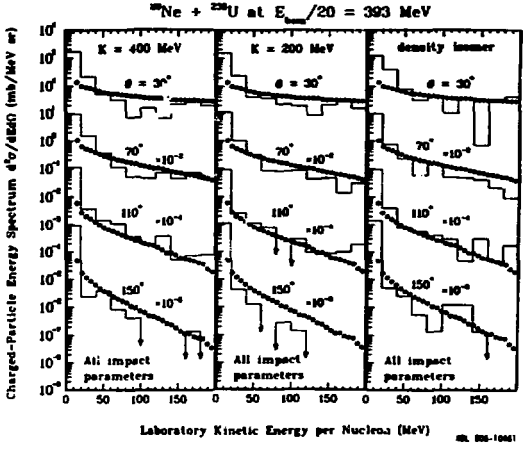

Fig. 3. Comparison of charge inclusive data[16]) (dots) with hydrodynamic results[15]) (histogram) for the three equations of state in fig. 2. All impact parameters are summed over.

motion[18]) and billiard ball calculations[19]) also demonstrate the great insensitivity of the inclusive spectra to the equation of state.

It must be emphasized that this insensitivity to W_0 is at the level of a factor of 2! Any differences less than a factor of 2 cannot be determined because of large inherent numerical uncertainties in solving eq. (4). Our theoretical resolving power is simply too poor at this time to determine any feature of W_0 from impact parameter averaged inclusive data. This point is also demonstrated in fig. 4 where results of an intranuclear cascade calculation by Yariv and Fraenkel[20]) are compared with the same data[16]). In a cascade picture, $W_0 \equiv 0$, since only kinetic degrees of freedom are considered. Nevertheless, again within that same canonical factor of 2-3, the calculations provide as fair a description of the data as hydrodynamics in fig. 3.

Given our limited calculational abilities, the best way to proceed is to consider a more restricted class of reactions for which the sensitivity to W_0 may be greater. Therefore, we turn next to central collisions.

A major experimental advance in the past two years has been the acquisition of the first data[21]) on central collisions. For those data, the associated charged particle multiplicity per event was required to be among the highest 15% of the multiplicity distribution. From detailed intranuclear cascade calculations[20]), this multiplicity cut corresponds to the range of impact parameters $b < b_{max} = 4 \cdot 1$ fm. For Ne+U the fraction of

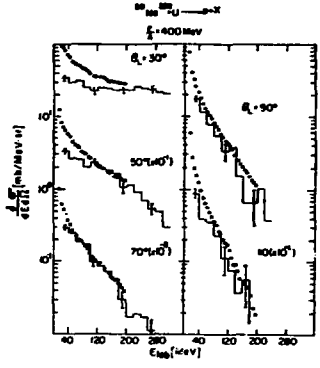

Fig. 4. Preliminary cascade calculations of Yariv and Fraenkel[20]) (histogram) compared to same data[16]) as in fig. 3.

the reaction cross section from impact parameters less than b_{max} is $(4/11)^2 \sim 15\%$. Therefore, the hydrodynamic results integrated up to b_{max} = 4 fm should be comparable with the data of Ref. [21]).

This comparison is shown in fig. 5. Note first that there does appear to be more sensitivity to the equation of state for central collisions. For example, at 30° the cross section falls off with energy slower for the softer $W_0(n)$, and at back angles there seem to be fewer low energy particles for the stiffer equation of state. Qualitatively we may attribute these effects to more complete stopping of Ne for the stiffer equation of state. For infinite stiffness, there would be no yield at 30° for central collisions while in the backward hemisphere high energy Ne fragments that bounced off the stiff U would be seen. Thus even with the large numerical uncertainties the qualitative trend of the calculations can be understood. However, we note again that thermal averaging is expected to reduce the differences among the three cases[17]).

There are two points to note in fig. 5. First, at 30°, where the hydrodynamic results are most sensitive to W_0, there is a large systematic discrepancy with data. Second, at larger angles, where the results are insensitive (modulo factor 2) to W_0, hydrodynamics provides a fair description of data as in fig. 3. We must conclude that even from centrally triggered Ne+U inclusive data, we still cannot determine W_0. As we shall see below, one problem is that $d^2\sigma/d\Omega dE$ still involves a ϕ average over possible reaction planes and this suppresses the sensitivity to W_0. However, the first point indicates that there is some essential physics missing at forward angles.

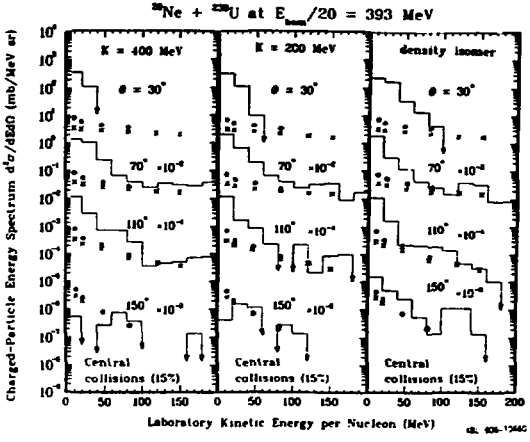

Fig. 5. Central triggered data[21]) compared with hydrodynamic results[15]) integrated from b = 0 to 4 fm.

The following three factors are thought to account for that large discrepancy at 30°. First, there are important nonequilibrium contributions to the forward yield. These nonequilibrium contributions arise because of finite mean free path and finite particle number effects[22]). Even at b = 4 fm, there are a few nucleons in Ne+U collisions that suffer only one or two binary NN scatterings which are forward peaked. Clear experimental evidence for the direct component has in fact been found in pp correlation studies[23]). It only takes a few direct scatterings to distort greatly the high energy (~200 MeV) forward yield. Second, the relationship between experimental multiplicity trigger and the impact parameter range $0 < b < b_{max}$ is not certain. Figure 6 shows the relation between the average associated multiplicity $\langle M \rangle$ for the experimental setup of Ref. 21) and the impact parameter b from the cascade calculations of Yariv and Fraenkel[20]).

The error bars indicate the large dispersion of the multiplicity distribution for fixed b. Therefore, in the highest 15% of the multiplicity distribution there is likely to be contribution from impact parameters b > 4 fm, which do not involve the complete geometrical overlap of Ne on U. These more peripheral collisions lead to increased forward yield at higher energies and also amplify the nonequilibrium contribution. Finally, there is a computational deficiency that may account for some of the discrepancy at 30°. The calculated results[15]) in fig. 5 do not include the thermal averaging over each fluid cell. That thermal averaging would broaden the 30° yield, increasing the higher energy cross sections.

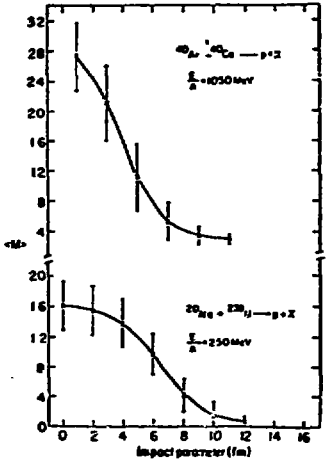

Fig. 6. Average associated multiplicity <M> and variance (error bars) for tag counter array used in Ref. [21]) for fixed impact parameter according to cascade calculations of Yariv and Fraenkel [20]).

What must we do in the future to gain sensitivity to $W_0(n)$? The first step is clearly to use heavier projectiles in order to reduce the nonequilibrium component. The average number of mean free path is R/λ = 1.6, 2.1, 3.7, for Ne, Ar, U respectively. Clearly Ne and Ar are too small to expect significant hydrodynamic effects. The goal experimentally will be U+U collisions by 1983. The second step will be to measure the reaction plane as well as <M> event by event. The importance of this is shown in fig. 7. Fig. 7 shows the first calculations of the triple differential cross sections, $d^3\sigma/dEdud\phi$, based on the hydrodynamic model of Ref. 24).

The unique hydrodynamic signature of Ar + Ca → 4 Jets is shown for b = 2 fm. One jet with ($\phi = 0^o$, $p_\perp \sim 0.3$ m, $y \sim y_{proj}$) is the bounced off remnant of the Ar projectile. The second jet with ($\phi = 180^o$, $p_\perp \sim 0.3$ m, $y \sim 0$) is the bounced off remnant of the Ca target. Finally, there are two jets squirted out perpendicular to the reaction plane ($\phi = 90^o$, $p_\perp \sim 0.3$ m, $y = y_{cm}$) arising from the compressed reaction zone. These jets are clearly visible in the triple inclusive cross section. However, when averaged over the orientation of the reaction plane, <ϕ>, the signature of these jets is washed away! Clearly we must determine the reaction plane via azimuthal correlations of charged fragments to gain sensitivity to hydrodynamic effects. It is important to emphasize in this regard

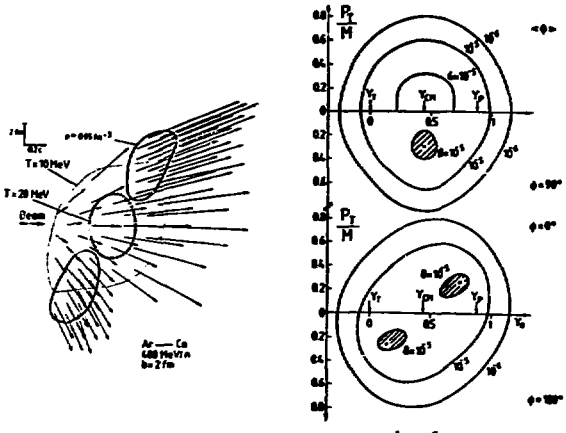

XBL 809-11619

Fig. 7. 3-D hydrodynamic calculations of Stöcker, et al.[2*]) for the triple differential cross section. The reaction Ar + Ca at b = 2 fm and E_{lab} = 400 MeV/A is considered. Contour plots for ϕ = 0°, 90°, 180° and averaged <ϕ> are shown as a function of rapidity y and transverse velocity $p_\perp/m$.

that such jetting phenomena are not found in cascade calculations[19]) and seem to be unique to hydrodynamics. Finally, it is obvious that to look for jets, multiparticle final states should be measured. A jet involves a strong correlation between groups of particles. While the triple differential cross section for a single fragment could indicate jetting by a peak at some (ϕ,θ,E), the jet signature would be amplified by measuring multiparticle distributions. This amplification is a simple consequence of taking a peaked distribution to some higher power. Thus, in future experiments, it would be most advantageous to make exclusive particle measurement.

Exclusive particle identification, when the number of charged fragments approaches 200, requires novel and innovative experimental techniques. Fortunately, the experimentalists are meeting the challenge. In fig. 8, two elaborate new devices, HISS[5]) and the Ball-Wall[26]), are illustrated. HISS is a two meter diameter by one meter gap 30 kiloGauss superconducting spectrometer. It will be able to measure exclusive projectile fragmentation for the first time. The ball consists of ~800 ΔE-E telescopes that measure exclusive target fragmentation. Together with the Wall array for

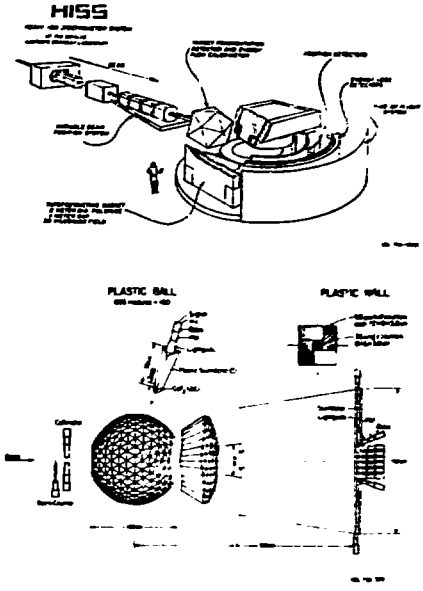

Fig. 8. Schematic layout of exclusive charged fragment experiments HISS[25]) and Ball-Wall[26]) under construction.

time of flight measurements, this system will be ideal for looking for hydrodynamic jets.

While we have not been able to extract properties of $W_0(n)$ as yet from data, the direction for future effort on this front is now clear and well under way.

3. Puzzling projectile fragments

I will now turn to the second topic concerning searches for new or unusual excited states of nuclear matter that are produced in nuclear collisions.

Since early cosmic ray studies, there have been recurring observations[27]) in emulsions of anomalous projectile fragments with much larger cross sections than expected geometrically. In contrast, the measured reaction mean free paths of primary incident nuclei with charge $2 \leq Z \leq 26$ and energy between 0.2 and 2 GeV/nucleon are perfectly consistent with simple geometrical

overlap models of the reaction cross section[28]. It is the secondary fragments produced in a nuclear collision that seem to have a component with a much smaller mean free path.

In a new experiment, Friedlander, et al.[29] have studied the subsequent interactions of secondaries and even tertiaries in sequential interactions in Em. Fig. 9a shows a "typical" event chain in this study. An incident Fe beam at 1.88 GeV/nucleon interacts with an emulsion nucleus (AgBr) losing two charges. The Cr (Z = 24) fragment continues in the emulsion until it too interacts, this time losing four charges. This tertiary Ca fragment then suffers yet another collision leaving a fourth

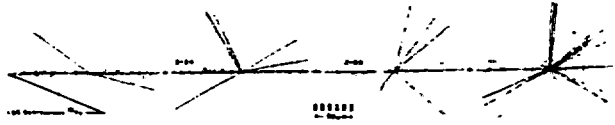

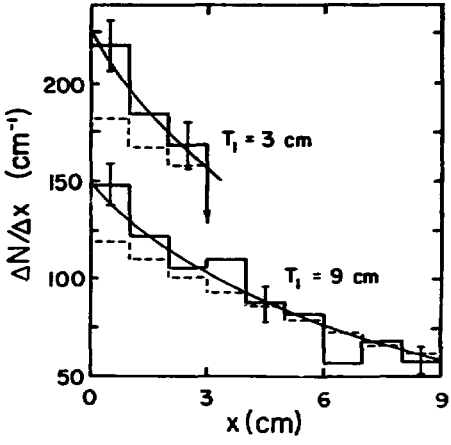

XBL 806-10262

Fig. 9. (a) Incident Fe (1.88 GeV/A) fragments four times in an emulsion[29].
(b) Observed distribution[29] of distances x between primary and secondary vertices (solid histogram). Expected distribution (dashed histogram) based on geometrical cross sections. Solid line assumes 6% secondaries have 10x geometrical cross section.

generation projectile fragment with Z = 11 to interact once more before leaving the emulsion as an α particle. Such multichain events are rare, but seem to occur more often than we would expect if all projectile fragments had normal geometrical mean free paths. Quantitatively, fig. 9b shows the number of secondaries that suffer a nuclear collision a distance x from the primary interaction vertex. Two classes of events are plotted. One is where the potential path length from the primary vertex to the end of the emulsion is larger than T_1 = 3 cm. The other is where that potential length is greater than T_1 = 9 cm. The solid histogram with error bars is the observed frequency. The dashed histogram is the expected distribution if all secondaries had geometrical cross sections. There is a clear excess of events with small mean free paths with x < 3 cm.

To try to account for the observation, a minimum χ^2 fit was made (solid curve) assuming that some fraction f of the secondaries had an anomalous cross section $E\sigma_{geom}$. The best fit was obtained with f = 0.06 and E = 10! Ten times geometrical cross section cannot be any familiar nuclear excitation. Furthermore, decays in flight were ruled out by requiring target fragments to be seen in each reaction. Thus, if this component is indeed real, it would indicate a new type of nuclear excitation with lifetime $\tau > 10^{-19}$ sec with a force field of much larger range than we are familiar with in nuclei.

Many conventional possibilities such as pionic atoms, hyperfragments, isotopic effects, resolution of multiparticle fragmentation, etc., have been ruled out[28]. Possible systematic experimental biases are, however, more difficult to evaluate. In any case, these observations remain as an intriguing puzzle to pursue in the future.

With the HISS spectrometer in fig. 8a it will be possible to analyze exclusive projectile fragmentation in the near future. If there are exotic nuclear excitations, then by searching for bumps in the invariant mass distribution $M^2 = (\Sigma p_i)^2$, it should be possible to identify them. For such an analysis the four momentum of <u>all</u> projectile fragments has to be measured. If the new state has a decay mode to all charged fragments, then HISS will be able to reconstruct the mass of that state.

4. An "almost" test of pion condensation

The final topic I will discuss is how relativistic nuclear collisions could be used to test for pion condensation at densities between 2-3n_0. As we saw in fig. 1, it is possible that for short times at least, $\Delta t \sim 3\text{-}5 \times 10^{-23}$ sec, some part of the nucleus could be compressed beyond the critical density for pion condensation. Our problem then is to identify what signatures such a phase transition would lead to experimentally. I propose below that we look for the transient, coherent pion radiation associated with the <u>onset</u> of pion condensation.

Our first expectation[6,7] is that pion condensation will lead to a softening of the equation of state $W(n,T)$ in eq. (4). However, there are two problems here. First there may not be enough time for the condensate to reach equilibrium. Second, the softening, ΔW, may be too small to detect. An estimate of the growth rate of the spin-isospin wave, $J_{\mu 5}(x) = \langle \bar{\psi}\gamma_\mu\gamma_5\psi(x)\rangle$, associated with pion condensation can be obtained by solving for the <u>complex</u> singularities of the pion propagator,

$$\Delta_\pi^{-1}(\pm i\gamma(\underset{\sim}{k}),\underset{\sim}{k}) = 0 \quad . \tag{7}$$

Eq. (7) was solved in Ref. 29) for two freely interpenetrating nuclear beams corresponding to the initial diving phase of nuclear collisions. Linear response theory then tells us that $\gamma(\underset{\sim}{k})$ is the growth rate of mode $\underset{\sim}{k}$, and hence $J_{\mu 5}(\underset{\sim}{x},t) \propto \gamma(\underset{\sim}{k})t\exp(i\underset{\sim}{k}\underset{\sim}{x})$ initially. In Ref. 29) we found that $\gamma(k) \sim (0.1\text{-}0.2)m_\pi \sim (5\text{-}10$ fm/c$)^{-1}$ for modes with $k \sim 2m_\pi \pm m_\pi$ oriented perpendicular to the beam axis. On the other hand, the diving phase of the collision only lasts[18]) $\Delta t \sim 5$ fm/c $\sim 1/\gamma(k)$, so that there is not likely to be enough time to reach the fully relaxed condensate. Furthermore, even if there were enough time, then the change in the equation of state may be too small. In fig. 10, we show the

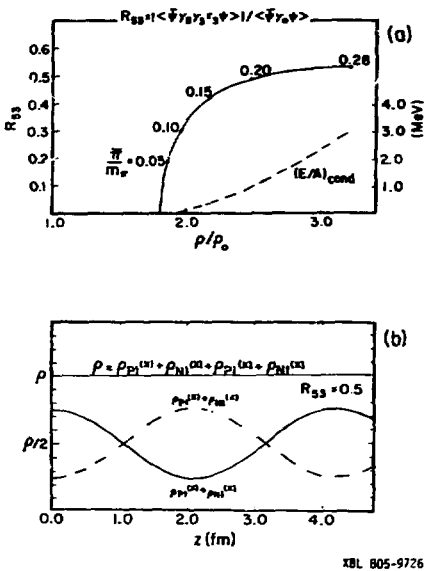

Fig. 10. a) The amplitude R_{33} of the spin-isospin density as function of density. The condensate energy, (E/A)cond, is also shown. b) Schematic plot of spin-isospin wave for $R_{33} = 0.5$.

results of a recent calculation[30]) of pion condensation in a mean field theory that was constrained by bulk nuclear properties for the first time. Unlike previous calculations of the condensate energy in chiral models[6,7]) we find that the condensate energy is indeed small, $|\Delta W| < 10$ MeV. As we saw in section 2, we are not

yet even sensitive to $\Delta W \sim 50$ MeV at this time. We conclude that the indirect consequences of the small softening of W are unlikely to be observable.

However, there is another feature of the onset of condensation that may be observable. That is the transient growth of spin-isospin wave toward the static equilibrium value shown in fig. 10. The point is that the axial current, $J_{\mu s}(x)$, is a source of pions

$$(\Box + m_\pi^2)\,\pi(x) = g_\pi \partial^\mu J_{\mu s}(x) \quad . \tag{8}$$

In equilibrium, $J_{\mu s}(\underset{\sim}{x},t) = J_{\mu s}(\underset{\sim}{x}) \propto \exp(i\underset{\sim}{k}_c\underset{\sim}{x})$ is independent of time, and no pions can be radiated. However, in the dynamical case of nuclear collisions $J_{\mu s}(\underset{\sim}{x},t) \propto \gamma t$ can acquire a time dependence as it grows toward the equilibrium value. Just as a time dependent charge current leads to photon radiation, eq. (8) tells us that a macroscopic growing axial current will radiate pions.

To compute the number of pions radiated, we note[31]) that for a classical source, $j(x) = \langle g_\pi \partial^\mu J_{\mu s}^- \rangle$, the solution of eq. 8 is a <u>coherent</u> state

$$|\pi^-{}_{out}\rangle = e^{-\bar{n}_o/2} \exp\left[i\int d^3k\, j(k)\, a^+(k) \right] |0\rangle \quad , \tag{9}$$

where $j(k)$ is the on-shell ($\omega_k = (k^2 + m_\pi^2)^{1/2}$) Fourier transform of $j(x)$:

$$j(k) = \int d^4x \frac{e^{i\omega_k t - i\underset{\sim}{k}\underset{\sim}{x}}}{(2\omega_k (2\pi)^3)^{1/2}}\, j(\underset{\sim}{x},t) \quad , \tag{10}$$

and $\bar{n}_o$ is the average number or π^- radiated:

$$\bar{n}_o = \int d^3k\, |\, j(k)\,|^2 \quad . \tag{11}$$

To estimate $\bar{n}_o$ we need a model for $j(\underset{\sim}{x},t)$. For a given condensate wave number $\underset{\sim}{k}_c$, we deduce[30]) from fig. 10 that

$$j(\underset{\sim}{x},t) \xrightarrow[t\to\infty]{} j_\infty(\underset{\sim}{x}) = g_\pi k_c R_{53} \rho \exp(i\underset{\sim}{k}_c\underset{\sim}{x}) \quad , \tag{12}$$

where $R_{53} \approx 1/2 - 1$, $k_c \approx 2m_\pi$, $g_\pi \approx m_\pi^{-1}$, $\rho \approx m_\pi^3$. However, this asymptotic value is reached only for $t \gg 1/\gamma(k_c)$. Initially, $j(\underset{\sim}{x},t) \propto \gamma(k_c)t$. Furthermore, we must modulate j by an envelope confining $j(\underset{\sim}{x})$ to the nuclear radius R and collision time Δt. Thus, we consider the following model[32])

$$j(\underset{\sim}{x},t) = j_\infty(\underset{\sim}{x})\,\theta(t)\,(1 - e^{-\gamma(k_c)t})\, e^{-x^2/2R^2}\, e^{-t/\Delta t} \quad . \tag{13}$$

Inserting into eq. (10) and noting that $\omega_{kc} \gg \gamma(k_c)$, $1/\Delta t$, we obtain the single π^- inclusive distribution for a fixed condensate mode $\underset{\sim}{k}_c$ as

$$|\, j(\underset{\sim}{k})\,|^2 \approx A^2 \frac{g_\pi^2 k_c^2}{2(2\pi)^3} R_{53}^2 \frac{\gamma^2(\underset{\sim}{k}_c)}{\omega_k^5} e^{-(\underset{\sim}{k}-\underset{\sim}{k}_c)^2 R^2} \quad , \tag{14}$$

where A is the number of interacting nucleons related to R via $\rho = A/(2\pi R^2)^{3/2}$. Integration over k in eq. (11) gives the average number of coherently radiated π^- as

$$\frac{\bar{n}_o}{A} \approx \frac{g_\pi^2 k_c^2}{4\sqrt{2}} R_{53}^2 \rho \frac{\gamma^2(k_c)}{\omega_{kc}^5} \sim 10^{-4}, \tag{15}$$

where we used $R_{53} = 0.5$, $k_c = 2m_\pi$, $\rho = 2n_0 = m_\pi^3$, $g_\pi = m_\pi^{-1}$, $\gamma = 0.2m_\pi$, and $\omega_{kc} = 2.2m_\pi$ to get the order of magnitude estimate. This is an extremely small number! Experimentally[1], the observed number of π^- at energy E per nucleon is

$$\left(\frac{n_{\pi^-}}{A}\right)_{exp} \approx 0.04 \frac{E}{m_N} \sim 400 \frac{\bar{n}_o}{A} \frac{E}{m_N} \quad ! \tag{16}$$

There is certainly no copious pion production associated with pion condensation. Of course, most pions are produced in incoherent inelastic $NN \to N\Delta \to NN\pi$ scatterings at these energies.

How can we hope to detect such a small signal? Consider the differential inclusive π^- cross section. From eq. (14), the pions produced coherently for a given mode k_c emerge with momentum $k \approx k_c \pm 1/R$. For large sytems, $1/R \ll k_c$, and the coherent pions are then almost monochromatic. However, from event to event the orientation of k_c will be randomly distributed according to the partial widths $\gamma(k_c)$. Performing this weighted average over k_c, the invariant single π^- inclusive cross section can be simply written as

$$\omega \frac{d^3\sigma}{dk^3}\Big)_o \approx \sigma_o \bar{n}_o \frac{\gamma^3(k)}{\int \frac{d^3k'}{\omega_{k'}} \gamma^3(k')} \quad . \tag{17}$$

It would be more accurate to use $k^2\gamma^3(k)/\omega_k^3$ in place of $\gamma^3(k)$ in eq. (17), but we are interested here in the qualitative features of coherent radiation. The essential point is that $\omega d^3\sigma/dk^3)_o \neq 0$ only for those k for which $\gamma(k) \neq 0$. In Ref. 29), we found that $\gamma(k) \neq 0$ only for $m_\pi \lesssim k_\parallel \lesssim 3m_\pi$ and $-m_\pi \lesssim k_\perp \lesssim m_\pi$. This is a toroidal domain of k perpendicular to the beam axis. Qualitatively, we can write in the cm frame

$$\omega \frac{d^3\sigma}{dk^3}\Big)_o \approx \sigma_o \bar{n}_o \frac{\omega}{(2\pi)^2 m_\pi^3} \exp\left[-[k_\parallel^2 + (k_\perp - 2m_\pi)^2]/m_\pi^2\right] \quad . \tag{18}$$

What remains now to be specified is the reaction cross section σ_o. An upper bound for this for A + A collisions is

$$\sigma_o \lesssim \pi(2R - \lambda_c)^2 \quad , \tag{19}$$

where $\lambda_c = 2\pi/k_c \approx 4.4$ fm is the wavelength of the spin-isospin wave and $R \approx 1.2A^{1/3}$ is the nuclear radius. Eq. (19) follows from the requirement that only those impact parameters contribute for which the transverse overlap dimension exceeds the wavelength λ_c of the spin-isospin wave. This gives $\sigma_o \approx 140$, 460, 3400 mb for Ne + NaF, Ar + Ca, U + U collisions respectively. To estimate n_o = 0.003, 0.006, 0.03 respectively, we assume that the average number of participants is about one-half the total number of nucleons. Finally, we can estimate the peak value of the invariant π^- cross section due to the <u>onset</u> pion condensation as

$$\omega \frac{d^3\sigma}{dk^3}(k_\parallel = 0,\ k_\perp \approx 2m_\pi) \approx 1,\ 7,\ 300\ \frac{mb}{(GeV)^2}c^3 \qquad (20)$$

for A + A collisions with A = Ne, Ar, U respectively. These are, of course, only order of magnitude estimates. More exact estimates would require inclusion of competing effects from pion absorption and optical dispersion $(\omega(k_c) < (k_c^2 + m_\pi^2)^{1/2})$.

The signature of this coherent radiation in Ne + NaF would thus be an 1 mb/GeV^2 bump at $\theta_{cm} = 90^o$, $k_\perp \approx 2m_\pi$. Could we observe such a tiny bump? In fig. 11 the invariant π^- cross section at $\theta_{cm} = 90^o$ as measured by Nagamiya, et al.[33] is shown for Ne + NaF at different bombarding energies.

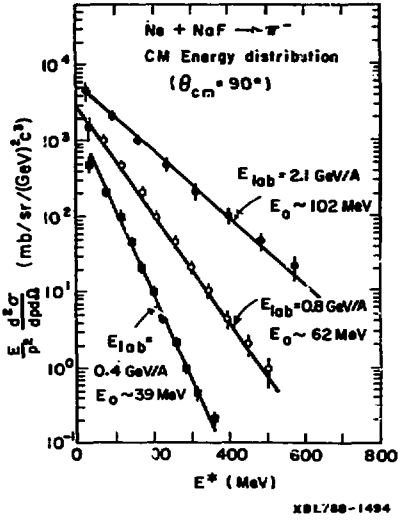

Fig. 11. Invariant π^- inclusive cross section[33] at $\theta_{cm} = 90^o$ as function of π cm kinetic energy. Reactions of Ne with 0.4, 0.8, 2.1 GeV/nucleon on NaF are shown.

Clearly, above 1 GeV/nucleon the background due to incoherent processes dominates for all E^*. However, as the beam energy is lowered to 400 MeV/nucleon, the incoherent contribution decreases dramatically. It still is ~10 mb/GeV^2 at $E^* = 200$ MeV, but it is almost at the level where a 1 mb/GeV^2 bump could be observable! Obviously, the crucial experiment is at even lower energies ~200 MeV/nucleon where the background due to incoherent pions could fall well below the 1 mb/GeV^2 level at $E^* = 200$ MeV.

Therefore, I propose the following test for pionic instabilities at densities $\sim 2n_0$: Scatter two equal mass nuclei (A + A) with A as big as possible (U + U) to increase the coherent cross section and to reduce finite size effects. Study the high k_i ($E^* > 200$ MeV), $\theta_{cm} = 90^0$ pion inclusive cross section as the beam energy is lowered to $E/A \sim 100$-200 MeV/nucleon. The signature of the transient coherent π radiation would be a break in the slope of the invariant cross section around $E^* \sim 200$ MeV. If no break is found, at least a strong upper bound on the growth rates of pionic instabilities will be obtained. By varying A and E/A, we should be able to find the needle in the haystack--if there is one.

5. Concluding remarks

Relativistic nuclear collisions offer a unique opportunity to probe properties of nuclear matter in completely uncharted domains of high density and temperature. However, we have found in the past few years that it is far from easy to read those properties off from actual data. Part of the difficulty was that we did not appreciate just how complex the basic reaction mechanism was in such collisions. Partly, we did not have clear ideas of what signatures to look for. There has been tremendous progress on both fronts. With the immense volume of data and calculations[1-4] available now, we have gained a much better understanding of the constraints imposed by geometry and phase space, the multicomponent nature of inclusive yields (direct, intermediate, thermal, fragmentation), and the distortions due to final state interactions such as composite production, Coulomb and nuclear shadowing. We have learned that the bulk of the data can in fact be understood in terms of intranuclear cascading[1,5,19,20], (multiple incoherent binary NN collisions) with initial state (Fermi motion) and final state interactions. Of course, many topics need further clarification, and basic reaction mechanism studies must continue. However, with our present knowledge we have also gained a better sense of which directions and observables to pursue in the future toward the goal of learning about high density nuclear matter. In this brief overview, I have discussed a few of those directions. Many other directions still need to be worked out as we chart this frontier of high densities and temperatures.

Acknowledgments

Inspiring discussions with H. Stöcker, H. Pugh, N. Glendenning, and P. Siemmens are most gratefully acknowledged. I have also profited from numerous discussions with S. K. Kauffmann, J. Knoll, R. Nix, A. Bodmer, E. Halbert, J. Cugnon, Z. Fraenkel, H. Gutbrod, R. Stock, S. Nagamiya, and E. Friedlander. This work was supported by the Office of Nuclear Physics of the U.S. Department of Energy under contract W-7405-ENG-48.

References

1) M. Gyulassy, "Relativistic Nuclear Collisions: Theory", LBL-11040 preprint, Proc. INS Kikuchi Summer School on Nuclear Physics at High Energies, Fuji-Yoshida, Japan, July 1-4, 1980.
2) H.H. Gutbrod, "Search for Collective Phenomena in Relativistic Nuclear Collisions," LBL-GSI preprint, Proc. INS Kikuchi Summer School, ibid.
3) S. Nagamiya, "Central Nuclear Collisions--Past and Future," LBL-10956 preprint, Proc. Hakone Seminar on High Energy Nuclear Interactions and Properties of Dense Nuclear Matter, Hakone, Japan, July 7-11, 1980.
4) L. S. Schroeder, "Pion Production in Nucleus-Nucleus Collisions Below a Few GeV/Nucleon," LBL-10899 preprint, Proc. Hakone Seminar, ibid.
5) K.K. Gudima, V.D. Toneev, Dubna JINR preprint E2-12624 (1979).
6) A.B. Migdal, Rev. Mod. Phys. 50 (1978) 107.
7) W. Weise, G.E. Brown, Phys. Reports 27C (1976) 1.
8) T.D. Lee, Rev. Mod. Phys. 47 (1975) 267.
9) J.I. Kapusta, Nucl. Phys. B148 (1979) 461, and refs. therein.
10) V. Ruck, M. Gyulassy, W. Greiner, Z. Phys. A277 (1976) 391.
11) G.G. Bunatjan, Yad. Fiz. 29 (1979) 258; Sov. J. Nuc. Phys. 30 (1979) 131.
12) J.R. Nix, Prog. Part. Nucl. Phys. 2 (1979) 237.
13) H. Stöcker, J.A. Maruhn, W. Greiner, Z. Phys. A293 (1979) 173; Phys. Rev. Lett. 44 (1980) 1846.
14) H.H.K. Tang, C.Y. Wong, Phys. Rev. C21 (1980) 1846.
15) J.R. Nix, D. Strottmann, A. Sierk, Preprint LA-UR-80-1280 (April 1980), in Proc. Hakone Seminar, ibid.
16) A. Sandoval, et al., Phys. Rev. C21 (1980) 1321.
17) P. Danielewicz, Nucl. Phys. A314 (1979) 465.
18) A.R. Bodmer, C.N. Panos, A.D. MacKellar, Argonne preprint, Phys. Rev. C in press.
19) E.C. Halbert, ORNL preprint (1980).
20) Y. Yariv, Z. Fraenkel, Phys. Rev. C20 (1979) 2227; and to be published.
21) R. Stock, et al., Phys. Rev. Lett. 44 (1980) 1243.
22) J. Knoll, Phys. Rev. C20 (1979) 773.
23) S. Nagamiya, et al., Phys. Lett. 81B (1979) 147.
24) H. Stöcker, et al., GSI preprints 9, 22 (1980).
25) Conceptual Design Report, Lawrence Berkeley Lab Pub 5004 (1978).
26) M.R. Maier, H.G. Ritter, H.H. Gutbrod, IEEE Trans. on Nuclear Science, Vol. NS-27 (1980) 42.
27) B. Judek, Can. J. Phys. 46 (1968) 343.
28) E.M. Friedlander, R.W. Gimpel, H.H. Heckman, Y.J. Karant, B. Judek, E. Gansauge, LBL-11136 preprint (1980).
29) M. Gyulassy, W. Greiner, Ann. Phys. 109 (1977) 485.
30) B. Banerjee, N.K. Glendenning, M. Gyulassy, LBL-10572 preprint (1980), Nucl. Phys. A, in press.
31) M. Gyulassy, S.K. Kauffmann, L.W. Wilson, Phys. Rev. C20 (1979) 2267.
32) M. Gyulassy, LBL-10883 preprint (1980), Hakone Seminar, ibid.
33) S. Nagamiya, et al., Proc. 4th High Energy Heavy Ion Summer Study, LBL-7766, UC-34C, CONF-780766 (1978) 97.